Molecular Dynamics Simulations of Methane Hydrate Decomposition†

Evgeniy M. Myshakin,*,‡,|| Hao Jiang,§ Robert P. Warzinski,‡ and Kenneth D. Jordan§

National Energy Technology Laboratory, U.S. Department of Energy, P.O. Box 10940, Pittsburgh, Pennsylvania 15236, Department of Chemistry and Center for Molecular and Materials Simulations, University of Pittsburgh, Pittsburgh, Pennsylvania 15260, and Parsons, South Park, Pennsylvania 15129

Received: August 12, 2008; Revised Manuscript Received: November 26, 2008

Molecular dynamics simulations have been carried out to study decomposition of methane hydrate at different cage occupancies. The decomposition rate is found to depend sensitively on the hydration number. The rate of the destruction of the cages displays Arrhenius behavior, consistent with an activated mechanism. During the simulations, reversible formation of partial water cages around methane molecules in the liquid was observed at the interface at temperatures above the computed hydrate decomposition temperature.

I. Introduction

Gas hydrates are crystalline inclusion compounds in which water cavities encage guest atoms or small molecules.[1] There are three main classes of hydrate structures: sI, sII,[2,3] and sH,[4] with the type of hydrate formed depending on the size and nature of the guest molecules. Methane hydrate formed under high pressure and at moderately low temperatures adopts the sI structure comprised of dodecahedral (5^{12}) and tetrakaidecahedral ($5^{12}6^2$) water cages with methane molecules occupying both size cages. The unit cell contains 46 water and 8 methane molecules at 100% occupancy.

Methane hydrate occurs in vast quantities in permafrost regions and oceanic sediments where cold temperatures and elevated pressures favor its formation.[1,5] Estimates indicate that the amount of gas in hydrates may be up to twice as large as the methane equivalent of all fossil fuel deposits and exceed conventional gas resources by an order of magnitude.[1] Such quantities may have profound implications for climate change and, if economically recoverable, energy supply. The natural release or production of methane from hydrate-bearing sediments involves decomposition of the solid hydrate to water and gas, typically by depressurization and/or thermal stimulation,[1] and transport of this to the ocean, atmosphere, or, in the case of production, a collection well. Methane hydrate decomposition relative to production processes has been studied by laboratory experiments[1,6−15] and field scale simulations have recently been published.[16−18]

Molecular dynamics (MD) and Monte Carlo simulations have proven especially useful for elucidating various properties of methane hydrate. For example, in a recent study from our group, MD simulations were used to investigate the thermal properties of methane hydrate and helped to validate new experimental values for thermal conductivity[19] and to provide insight into the reasons for its anomalous behavior as compared to ice.[20] Several MD and Monte Carlo (MC) simulations of methane hydrate formation and dissociation have been reported,[21−35] but many issues still remain to be resolved, with different studies often reaching different conclusions. Rodger and co-workers[30−32] analyzed methane hydrate formation during ~10 ns trajectory runs with the SPC force field[36] and found several occupied 5^{12} cages at the end of the simulations. They also used the local molecular harmonic model[30] to estimate critical cluster sizes for the nucleation of the methane hydrate crystal. Kuhs et al.[29] used MD simulations and the KKY force field[37] to study phase interface behavior of methane hydrate with water under temperatures below the KKY computed melting point of hexagonal ice (*Ih*). The thermal conditions employed in that study promoted rearrangements of adsorbed water molecules at the interface with a tendency to complement open cages. Rodger[26] studied methane hydrate decomposition using the SPC model under mild melting conditions, 15 to 20 K above the computed hydrate decomposition point, and found ice- and hydrate-like structures in the water phase; however, no significant clustering was observed. Báez and Clancy[23] performed MD simulations of methane hydrate particles containing up to 400 water molecules by using the SPC/E model[38] and found that hydrate decomposition proceeded in a stepwise manner and was determined by the decay of open cages at the hydrate interface. English et al.[25] used MD simulations with the polarizable TIP4P-FQ water model[38] to study spherical methane hydrate crystallites in contact with pure water and water−methane mixtures at $T = 277$ K and $P = 6.8$ MPa. These authors found that the decomposition rate does not depend strongly on the cage occupancy over the 80−100% occupancy range and that the rate-controlling step of the hydrate decomposition involves diffusion of methane molecules from the crystal surface into the liquid phase.

In the present work, thermally induced decomposition of methane hydrate in coexistence with liquid water is studied. The presence of a liquid phase at the interface removes the undesired effects of superheating or supercooling of the solid phase.[39,40] The coexistence method provides a straightforward way to determine the dissociation or melting point of an interface. The simulations are carried out with 100%, 95%, and 85% initial methane occupancy of the hydrate cages, and at a pressure of 6.8 MPa, which was previously used in experimental studies of methane hydrate dissociation at the National Energy Technology Laboratory (NETL).[8,9] The present simulations differ from those discussed above in that longer simulation times are employed and the force field used allows for explicit polarization of the water molecules. The information gained on the dependence of the rate of hydrate decomposition on the cage

‡ National Energy Technology Laboratory, U.S. Department of Energy.
|| Parsons.
§ University of Pittsburgh.
† Part of the "Max Wolfsberg Festschrift".
* Corresponding author. E-mail: evgeniy.myshakin@netl.doe.gov.

10.1021/jp807208z CCC: $40.75
Published on Web 01/07/2009

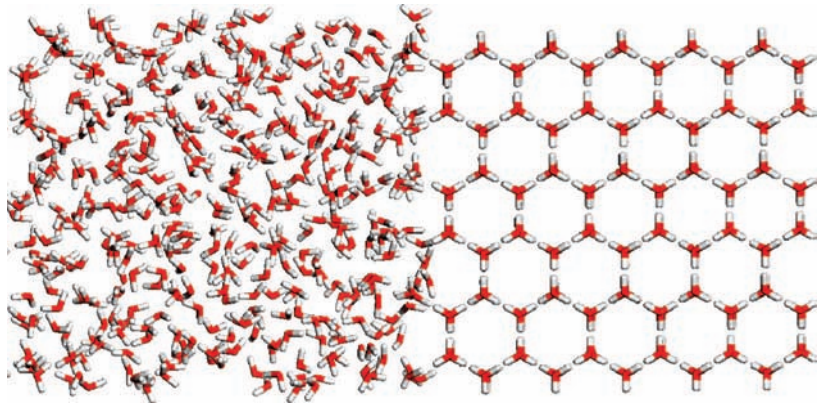

Figure 1. The initial simulation box used in the simulations of the melting of ice *Ih*.

occupancy could facilitate improvements in the kinetics experiments in models used to predict hydrate dissociation in sediments at laboratory and reservoir scale. Simulations were also carried out on the ice *Ih*/liquid water interface. These serve as a validation of the computational procedures.

II. Computational Details

i. Force Field. The charge-on-a-spring (COS/G2) force field[41] was used for water in both the hexagonal ice/water and methane hydrate/water simulations. This force field employs rigid monomers, positive point charges located on the H atoms, and a countering negative point charge on the so-called *M* site located on the rotational axis, displaced 0.22 Å toward the H atoms. Polarization is described by use of a mobile point charge attached harmonically to the *M*-site,[41] and Lennard-Jones (LJ) 12-6 interactions are employed between O atoms to account for short-range repulsion and long-range dispersion interactions between water molecules. The methane molecule was described by a rigid five-site nonpolarizable model, with partial charges located on the C and H atoms of methane to reproduce its electrostatic potential and a Lennard-Jones site located on the C atom. The charges and Lenard-Jones parameters for methane are from ref 42. The Lorentz−Berthelot combination rules[43] were used to determine the parameters for the Lennard-Jones interactions between the water and methane molecules. Ewald summation[44] was used to account for long-range electrostatic interactions. The Fourier part of the Ewald sums was evaluated by using the particle mesh Ewald method (PME) of Darden and co-workers.[45,46] The cutoff radius for the LJ interactions was chosen to be 9 Å for the hexagonal ice/water system and 10 Å for the methane hydrate/water system, with the corresponding switching distances being 7.5 and 8.5 Å. Due to the use of cutoffs for the LJ interactions, long-range dispersion corrections for energy and pressure were applied. The GROMACS package[47] was used to perform the MD simulations.

ii. Ice/Water Simulations. The preparation of the initial configurations for the hexagonal ice/water simulations was accomplished by use of NVT simulations, while the production runs were performed in the NPT ensemble. In the latter simulations, pressure was controlled by a Parrinello−Rahman barostat[48,49] with a relaxation time of 4 ps and temperature was controlled by a Nóse−Hoover thermostat[50,51] with a relaxation time of 2 ps. Use of the barostat allows the simulation box to readjust its dimensions in response to phase transformation. The simulation boxes were designed so that the melting occurs in the *z*-direction normal to the interface. A time step of 1 fs, which is small enough to avoid errors from the constraints, was used in the simulations of the hexagonal ice/water system.

The procedure of ref 52 was used to generate a hexagonal ice (*Ih*) sample with a dipole moment close to zero. The secondary prismatic {1 1 −2 0} plane, which is reported to be the fastest growing face of hexagonal ice,[53] was put in contact with the liquid water. The initial configuration had 432 water molecules in the solid phase and 438 water molecules in the liquid phase. The initial configuration was prepared by using a procedure analogous to that used for the methane hydrate/water system and described below. The last step in the preparation of the hexagonal ice/water system involved a 50 ps relaxation run in the NPT ensemble at a temperature of either 235 or 245 K and a pressure of 1 atm. This resulted in a simulation box with dimensions of about 22 × 23 × 54 Å^3. The simulation box was chosen to be orthogonal, although an orthorhombic presentation is also possible (Figure 1). Periodic boundary conditions (PBC) were applied in all directions, with the *z*-direction being taken normal to the solid/liquid interfaces. Thus, the ice slab is of infinite extent in the *x* and *y* directions and has two liquid interfaces. Given the anisotropy of the hexagonal ice crystal and the sizable density change that occurs upon melting of ice, anisotropic pressure coupling allowing independent fluctuations of the three box lengths was used in the simulations. The off-diagonal compressibility values were set to zero to retain a rectangular box. The production runs were carried out for 10 ns.

iii. Methane Hydrate/Water Simulations. In the simulations of methane hydrate decomposition, the hydrate crystal was comprised of structure I unit cells belonging to the cubic space group *Pm*3*n* with a lattice constant of 12.03 Å. A 4 × 3 × 3 supercell was created containing a total of 36 unit cells with near-zero net dipole moment and satisfying the Bernal−Fowler rules.[54] This supercell was then used to created the hydrate slab with infinite extent in *x* and *y* directions and two interfaces. Incomplete open cages, which promote decomposition at the beginning of the simulations, were introduced at the interfaces. Three methane hydrate models with 100%, 95%, and 85% cage occupancies were prepared (models 1, 2, and 3, respectively). Model 2 best represents the occupancy typical of naturally occurring methane hydrate, with the large and small cage occupations being chosen to be consistent with the experimental data reported by Sloan et al.[55] For Model 3, the distribution of methane between large and small cavities was computed by using eq 6 of ref 55, which connects the hydration number and large and small cage occupancies (Table 1). A liquid water layer consisting of 188 water molecules at a density of 1 g/cm^3 was then concatenated to the solid hydrate in the *z*-direction.

The simulation box under periodic boundary conditions was equilibrated by using the following procedure. The hydrate phase

TABLE 1: Cage Occupancies in the Hydrate Crystal and Number of Molecules in the Simulations

	% occup.	θ_L[a]	θ_S[a]	water in liquid	water in hydrate	methane	total molecules
model 1	100	1	1	1188	1296	243	2727
model 2	95	0.97	0.87	1188	1296	230	2714
model 3	85	0.87	0.77	1188	1296	206	2690

[a] θ_L, θ_S: fractional population of large and small cages, respectively.

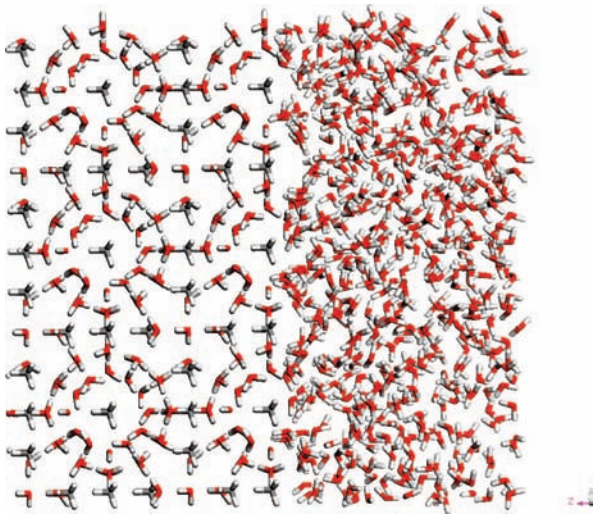

Figure 2. A portion of the initial simulation box representing the interface between the methane hydrate lattice and liquid water.

was frozen and MD simulations were run for 100 ps in the NVT ensemble at $T = 900$ K, allowing the liquid phase to be equilibrated. The water molecules in the liquid phase were then frozen, and the methane hydrate was allowed to equilibrate in an NVT simulation for another 50 ps at the temperature used in the subsequent production run. During this portion of the equilibration no diffusion of methane molecules from the open cages to the liquid was detected. This step was followed by a 50 ps NPT simulation of the entire system at the same temperature, $P = 6.8$ MPa, and using the weak coupling Berendsen thermostat and barostat[56] to readjust the box dimensions and to relax the solid/liquid interface. This resulted in simulation boxes of about $36 \times 36 \times 73$ Å^3 in size. A portion of the simulation box showing the solid/liquid interface is depicted in Figure 2. The numbers of water and methane molecules used in the simulations are reported in Table 1. The total numbers of molecules are 2727, 2714, and 2690 for models 1, 2, and 3, respectively. Below the ice point dissociation of methane hydrate is dictated by an "ice-shielding" mechanism in which the diffusion of methane molecules through a porous ice layer formed during the decomposition of hydrate is the controlling step.[57−60] In the present study, the lowest simulation temperature used for methane hydrate decomposition is significantly above the ice point associated with the COS/G2 force field, which avoids ice layer formation.

Production runs were carried out for 16 ns in the NPT ensemble, with *semiisotropic* pressure coupling permitting the z-dimension to fluctuate independently from the x and y directions. Pressure was controlled by a Parrinello−Rahman barostat[48,49] with a relaxation time of 4 ps and temperature was controlled by a Nóse−Hoover thermostat[50,51] with a relaxation time of 2 ps. A time step of 2 fs was used in the simulations.

iv. Analysis of Structures. To monitor the kinetics and to elucidate the mechanisms of melting of ice *Ih* and of methane hydrate decomposition, an algorithm employed previously by Báez and Clancy[23,61] and by English et al.[25,62] was used to identify whether individual water molecules are in the liquid and solid (ice or hydrate) phases. In this approach, an angular order parameter, F,

$$F_i = \sum_{j=1}^{n_i-1} \sum_{k=j+1}^{n_i} (|\cos \theta_{jik}|\cos \theta_{jik} + 0.11)^2 \qquad (1)$$

is calculated for each water molecule. In eq 1, n_i is the number of water molecules in the first solvent shell of the water molecule i, and j and k are indices running over these nearest neighbors, and θ_{jik} is the angle between the O atoms of the j, i, and k monomers. For molecule i there are $n_i(n_i - 1)/2$ independent triplet angles. For tetrahedral bonding, there are six angles and the cosine of the angle θ_{jik} is close to -0.33. Thus, F_i provides a measure of deviation from perfect tetrahedral coordination ($F = 0$) and serves to distinguish solid-like ($F < 0.4$) and liquid-like ($F > 0.4$) water molecules.[23−25,61,62] Further differentiation of ice-like and hydrate-like water molecules is based on identification of cyclic pentamers, which are present in the hydrate and absent in ice *Ih*. In hydrates water molecules participate in shared vertices of four, five, or six cyclic pentamers. Thus, a water molecule is considered to be ice-like if $F < 0.4$ and is not participating in any five-membered rings, and hydrate-like if $F > 0.4$ and forms part of four, five, or six cyclic pentamers.

After the initial assignment to liquid, ice, or hydrate phase, water molecules are reclassified according to the phase identity of their neighboring water molecules,[63] so that if a given water molecule has a phase identity different from that of three or more of its neighbors, the phase identity of the molecule in question is reassigned. A methane molecule having more than ten hydrate-like water molecules within a distance of 5.5 Å is considered to be a part of the hydrate crystal.[24] These criteria were found to provide a suitable recognition for bulk phases of hexagonal ice, methane hydrate, and liquid water.[23,61]

III. Results

i. Ice/Water. Figure 3 reports the total energies of the ice/water system during 10 ns simulations at $T = 235$, 240, and 245 K and $P = 0.1$ MPa. Simulations at $P = 6.8$ MPa gave nearly the same results as those at $P = 0.1$ MPa, in agreement with the weak experimental dependence of the melting point of *Ih* ice on pressure.[64] For the $T = 240$ and 245 K simulations, the energy is found to increase with time, reflecting the melting of ice.

Figure 4 reports the number of water molecules in the ice phase as a function of time for each of the three temperatures. At $T = 235$ K, the number of water molecules in the ice phase remains constant over time, except for small fluctuations about the average. However, at $T = 240$ and 245 K, significant decomposition of the interface of the ice crystal has occurred within 1 ns of simulation time. The interface movement is readily apparent from examination of its variation along the length of the simulation box. Figure 5 reports the density profiles averaged over 30 ps intervals at representative time points from

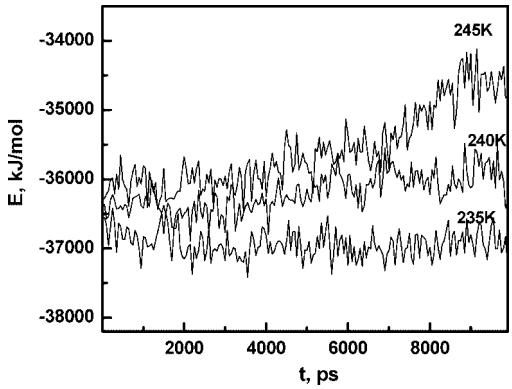

Figure 3. Total energy vs. time for NPT simulations of the ice/liquid water system at $P = 1$ bar and $T = 235$, 240, and 245 K.

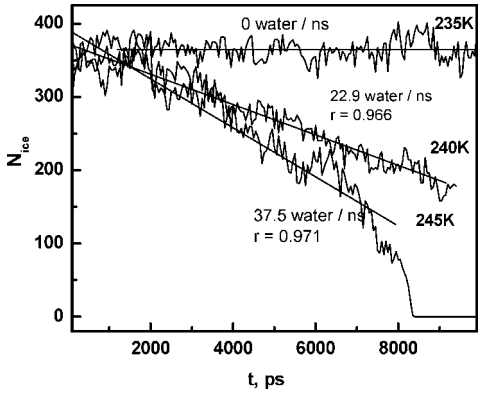

Figure 4. N_{ice}, the number of water molecules in the ice phase, as a function of time for the $T = 235$, 240, and 245 K simulations. The linear fits to the data are reported, with the lengths of the lines indicating the range of data employed in the fitting. The number of water molecules entering the liquid phase per nanosecond and the r values from the linear regression analysis are also reported.

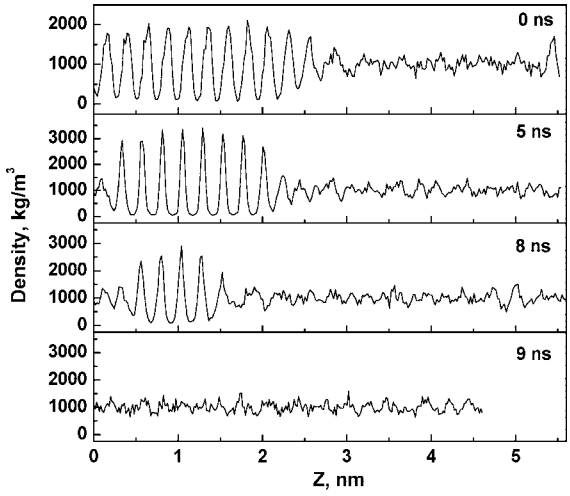

Figure 5. Density profiles along the simulation box of the ice/liquid water sample for the $T = 245$ K simulation. Densities (mean values averaged over 30 ps) are reported at the beginning of the simulation and after 5, 8, and 9 ns.

the $T = 245$ K simulation. It is clear from this figure that at $T = 245$ K, the solid ice phase has completely melted within 9 ns.

To more precisely determine the melting point (T_m) of ice as described by the COS/G2 model, simulations were carried out for a series of temperatures near 235 K. These simulations give a melting point of 236 ± 2 K, appreciably below the experimental value of 273.15 K. Table 2 reports the melting point of ice obtained with several common water models. From the table it is seen that the SPC/E and TIP4P models underestimate the melting temperature by even more than the COS/G2 model. The melting point obtained with the five-site TIP5P water model,[66] which was parametrized to accurately match the temperature of the density maximum of the liquid, is closest to experiment. Even though the COS/G2 model significantly underestimates the melting point of ice, it is more successful at predicting the decomposition temperature for methane hydrate, as will be shown in the next section.

TABLE 2: Melting Point (K) of Ice Obtained by Simulations with Direct Coexistence of the Solid and Liquid Phases Together with the Results from Free Energy Calculations and Gibbs−Duhem Integration

model	interface coexistence[a]	free energy[a]
SPC/E	213(2)[b]	215(4)[b]
TIP4P	229(2)[b]	232(2)[b]
TIP5P	271(2)[b]	274(6)[b]
COS/G2	236(2)[c]	

[a] The statistical uncertainties in the various calculations are indicated in parentheses. [b] Reference 65. [c] Present study.

ii. Methane Hydrate. The approach used above for ice was also employed to calculate the decomposition temperature of methane hydrate as described by the COS/G2 model, giving $T_{eq} = 268 \pm 3$ K at $P = 6.8$ MPa for 95% cage occupancy, in reasonable agreement with experimental values summarized by Sloan and Koh,[1] i.e., 282.6 K at 6.77 MPa. This is consistent with the conclusion of ref 67 that the COS/G2 water model provides a good description of methane hydrate. Calculations to determine the decomposition temperatures for the 85% and 100% cage occupancy cases were not undertaken as T_{eq} is not expected to depend strongly on the occupancy within a 85−100% range, and these values are not needed for the subsequent analyses.

The temperature dependence of methane hydrate dissociation was investigated by carrying out simulations at $T = 265$, 272, 277, 280, 290, and 300 K. The decomposition of the hydrate is characterized by a breakdown of the hydrogen bond network of the hydrate lattice and the diffusion of methane molecules from partially open cages into the liquid phase. These processes are evident from the evolution of the OO, CO, and CC radial distribution functions (RDFs). As shown in Figure 6, the structure in the RDFs associated with the methane hydrate lattice is gradually washed out, being essentially totally lost by 6 ns in the $T = 300$ K simulation. The peak at short distances in the C−C pair distribution function that increases with simulation time is a consequence of supersaturation of the liquid phase.

Figure 7 reports the number of methane molecules remaining in the hydrate phase as a function of time for the simulations at $T = 265$, 280, 290, and 300 K and for each of the three occupancies. Linear fits of the data are used to determine the rates of the methane hydrate decomposition. The data used for fitting were several nanoseconds in duration, from the beginning of a production run until the rates start oscillating or until the last stage of melting (for $T = 300$ K) (the reasons for the oscillations will be discussed below). From the average interface area of the moving plane between liquid and solid phases, it is straightforward to determine the rate of methane release in more usual units of moles of CH_4 per square meter per second. The results are reported in Table 3. Another convenient way to characterize crystal decomposition is to use the interface response function (IRF) introduced by Wilson and Frenkel.[68,69]

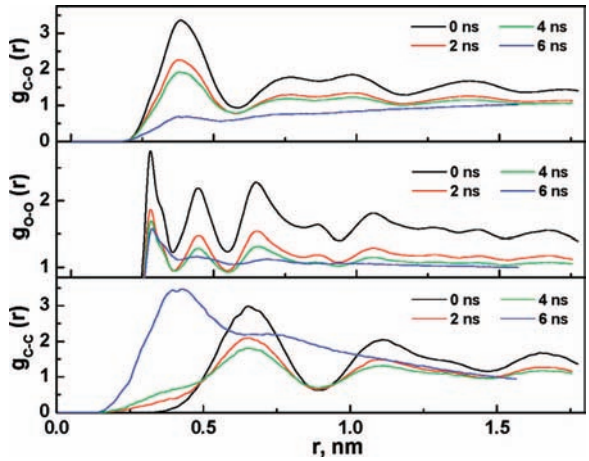

Figure 6. Carbon−oxygen, oxygen−oxygen, and carbon−carbon radial distribution functions for methane hydrate during decomposition at $T = 300$ K and 95% initial occupancy of the cages.

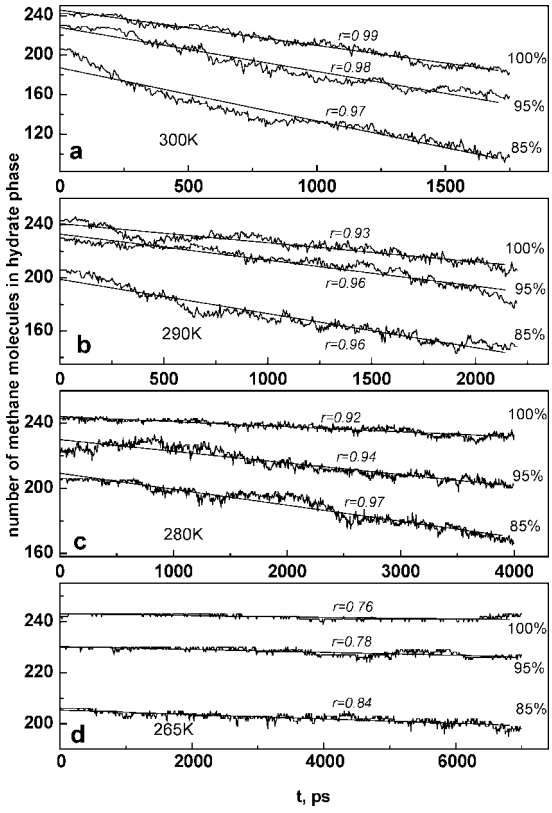

Figure 7. Numbers of methane molecules remaining in the solid hydrate phase as a function of time for the MD simulations at $T =$ 265, 280, 290, and 300 K are shown in parts a, b, c, and d, respectively. Linear fits to the data are depicted, and the r values from the linear regression analyses are reported.

The IRF is associated with the velocity at which the interface boundary moves as a function of a driving force (deviation from the decomposition temperature in this work). To determine the IRFs, the mass of methane hydrate decomposed per square meter per second was calculated by using the hydration number together with the corresponding computed densities of the bulk hydrate phase.

An alternative approach to defining the movement of the solid−liquid interface is based on the average order parameter profile along the Z direction.[70] To calculate the average order parameter profile, the simulation box is divided into a number of "slices". Within each "slice", each water molecule is assigned

TABLE 3: Rates of Methane Release ($R(CH_4)$) and Interface Response Function (IRF) for Different Temperatures and Cage Occupancies[a]

T, K	% occupancy	$R(CH_4)$, 10^3 mol/m^2 s	IRF, m/s
300	100	4.55 ± 0.38	0.63 ± 0.04 (0.61 ± 0.16)
	95	6.49 ± 0.39	0.94 ± 0.04 (0.80 ± 0.19)
	85	8.31 ± 0.39	1.32 ± 0.04 (1.05 ± 0.15)
290	100	1.55 ± 0.28	0.20 ± 0.03 (0.25 ± 0.11)
	95	2.55 ± 0.28	0.34 ± 0.04 (0.31 ± 0.15)
	85	3.36 ± 0.33	0.49 ± 0.03 (0.38 ± 0.09)
280	100	0.43 ± 0.20	0.05 ± 0.02 (0.04 ± 0.03)
	95	0.80 ± 0.21	0.10 ± 0.03 (0.07 ± 0.04)
	85	1.16 ± 0.23	0.16 ± 0.03 (0.11 ± 0.05)
277	100	0.20 ± 0.11	0.03 ± 0.02
	95	0.32 ± 0.12	0.04 ± 0.02
	85	0.79 ± 0.19	0.11 ± 0.02
272	100	0.13 ± 0.07	0.02 ± 0.01
	95	0.20 ± 0.13	0.03 ± 0.02
	85	0.30 ± 0.15	0.04 ± 0.02
265	100	0.03 ± 0.04	0.003 ± 0.01
	95	0.07 ± 0.08	0.01 ± 0.02
	85	0.10 ± 0.08	0.01 ± 0.01

[a] The IRFs obtained via the order distributions are given in parentheses.

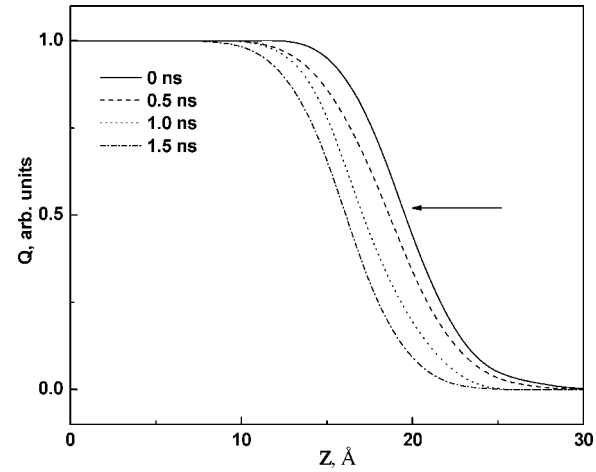

Figure 8. Order parameter distribution profiles of water molecules along the length of the simulation box of the hydrate sample with 100% initial occupancy during the decomposition reaction at $T = 300$ K. The curves were generated by using data from 20 ps averages around the indicated times. The arrow indicates the direction of the interface motion.

an order parameter of 1 for a molecule in the solid phase and 0 for a molecule in the liquid phase. Next, the sum of the order parameters for the individual water molecules is divided by the total number of water molecules in the "slice". The resulting average order parameter (Q) thus represents the fraction of water molecules in the solid phase. Figure 8 reports typical average order parameter profiles as a function of the z coordinate for snapshot configurations for initial cage occupation of 100% at $T = 300$ K. The results for each reported time (0, 0.5, 1.0, 1.5 ns) are averaged over 20 ps intervals. The Z positions (Å) corresponding to a 0.5 value of the average order parameter

profiles were used to evaluate the IRFs. Up to six sets of average order parameter profiles with different initial times were computed in each case to improve the statistics. The resulting IRFs for the $T = 280$, 290, and 300 K simulations are included in parentheses in Table 3. For the $T < 280$ K simulations, the average order parameter profiles obtained in this manner had large uncertainties and are not reported. From the results given in Figure 8, the thickness of the interface layer between the perfect hydrate crystal and the liquid phase is estimated to be 5−7 Å, in good agreement with a previous estimate of 5 Å.[1]

IV. Discussion

The results reported in Table 3 reveal a strong sensitivity of the dissociation rate on the cage occupancy. Depending on the temperature, a reduction of the cage occupancy from 100% to 95% causes a 50% to 90% increase in the long term rate of methane release. The introduction of empty cages in the methane hydrate crystal causes a destabilization of the lattice, which promotes quicker hydrate decomposition due to the greater instability of the empty cages compared to those containing methane.[1,25,62] A greater change in the decomposition rate is found when the cage occupancy is reduced from 100% to 95% than from 95% to 85%. These results confirm that the hydrate lattice with 100% occupancy of the cages is especially stable against decomposition. Introducing even a small number of empty cages greatly enhances the kinetics of the dissociation reaction. These results appear contradictory to those of English et al.,[25] who found in their simulations that the decomposition rate does not depend sensitively on cage occupancy (100%, 90%, and 80%). However, these authors considered the decomposition of relatively small 10−12 Å radius hydrate spheres, making their simulations more relevant as a model for decomposition of small hydrate nuclei rather than of bulk hydrate samples. We note also that the experimental decomposition conditions reported in the work of English et al. (276.65 K, 6.8 MPa) and employed in their simulations are well within the thermodynamic stability region for methane hydrate and are therefore in error.[1] Indeed, at $T = 276.65$ K, the equilibrium decomposition pressure reported in the literature is 3.7 MPa.[1] Finally, we note that English et al.[25] did not report T_{eq} for the TIP4P-FQ force field[38] used in their simulations, further hampering a comparison of their results with our data.

To describe the kinetics of hydrate dissociation Bishnoi and co-workers[10,11] proposed the following equation:

$$\frac{dX}{dt} = -A_s K_0 \exp\left(-\frac{\Delta E_a}{RT}\right)(f_e - f_s) \qquad (2)$$

This equation connects the total surface area (A_s), intrinsic reaction constant (K_0), temperature, activation energy (ΔE_a), and the fugacity of methane at equilibrium (f_e) and at the interface (f_s). From the experimental dependence of the decomposition rate on temperature, Bishnoi and co-workers[11] deduced a value of 81 kJ/mol for ΔE_a. Our calculated rates are plotted vs. T in Figure 9a. For the 100% and 95% occupancy cases, the rates display Arrhenius-like behavior for temperatures above 277 K. For the 85% occupancy case, Arrhenius behavior is seen for temperatures greater than 272 K. However, at $T < 277$ K for 100% and 95% occupancy, and $T < 272$ K for 85% occupancy, the dissociation rates depend linearly on temperature.

To elucidate the origins of this behavior and to analyze the cavity breakup process in more detail, the methane molecules are partitioned into three groups at the beginning of the simulations: those inside closed 5^{12} (small) cages, those inside closed $5^{12}6^2$ (large) cages, and those associated with incomplete

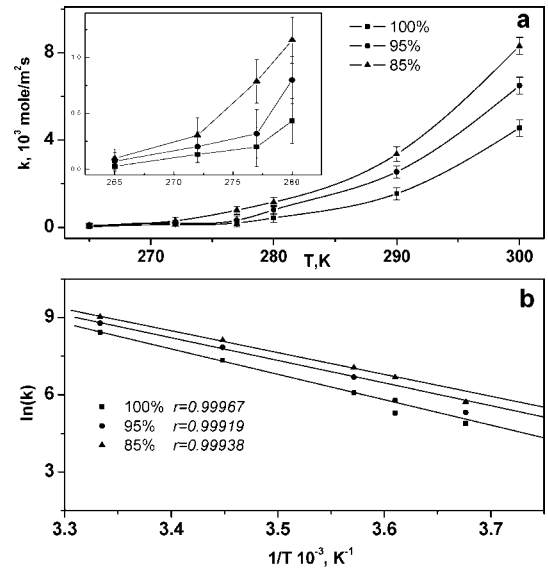

Figure 9. (a) Temperature dependence of **k**, the rate of methane release during hydrate decomposition, for initial 85%, 95%, and 100% cage occupancies. The insert shows on expanded scale the rates at the lower temperatures. (b) Arrhenius plot for methane hydrate decomposition. In determining the slopes, for 85% occupancy the $T = 277$, 280, 290, and 300 K data points were used, and for 95% and 100% occupancy, the $T = 280$, 290, and 300 K data points were used.

open cages at the interface. This partitioning is based on application of the recognition procedure described above to determine the number of hydrate-like water molecules within 5.5 Å of a particular methane molecule. A methane molecule is assigned as inside a large cage if it is surrounded by 23 or 24 hydrate-like water molecules, and inside a small cage if it is surrounded by 19 or 20 hydrate-like water molecules. The remaining methane molecules are considered to be trapped at the interface in open cages. This assignment is done once and a further procedure monitors the number of hydrate-like molecules within 5.5 Å of a methane molecule. As soon as that number falls below 10 a corresponding cage is considered to be destroyed. This approach allows us to determine separate decomposition rates for large, small, and open cages with guest molecules.

Figure 10 reports the number of methane molecules in closed 5^{12} and $5^{12}6^2$ cages and in incomplete open cages at the interface as a function of time and temperature. For low temperatures (i.e., $T = 277$ K for models 1 and 2 and $T = 272$ K for model 3), the closed hydrate cages essentially remain intact during the entire 16 ns simulation time, and the kinetics is determined by the methane molecules initially residing in open cages at the interface (compare parts d and e of Figure 10). Obviously, for sufficiently long simulation times, decomposition of the closed hydrate cages would be observed at these temperatures. Inspection of the low temperature trajectories and the average order parameter profiles (to locate the position of the interface boundary) also confirms that the growing concentration of methane molecules in the liquid is due to methane molecules initially located at the interface. The switchover from linear to exponential temperature dependence of the rate occurs at the temperature at which the dissociation of the closed hydrate cages becomes apparent in the simulations. The switchover temperature is lowest for the 85% occupancy case because of the destabilization of the lattice caused by the methane vacancies.

These results show that there are two regimes of hydrate decomposition, one characterized by diffusion of methane molecules out of partially broken (open) cages at the interface,

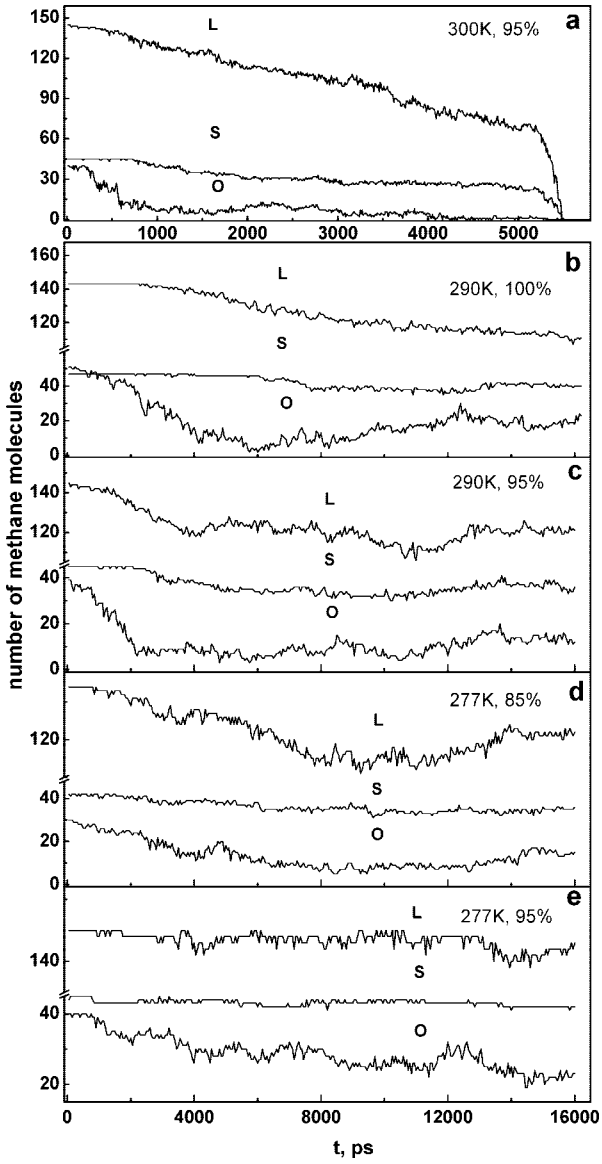

Figure 10. Evolution of hydrate cages during simulations under different conditions. The curves labeled "L" and "S" report respectively the number of methane molecules in large $5^{12}6^2$ and small 5^{12} cages of the hydrate lattice. The curve labeled "O" reports the number of methane molecules in open cages at the interface.

accompanied by decomposition of these cages, and displaying a linear dependence of the dissociation rate on temperature, and the other characterized by the further decomposition of the hydrate crystal involving the closed cages and demonstrating Arrhenius-like behavior of the rates. Escape of the methane from the open cages occurs with no or very low barrier, whereas decomposition of the water cages is associated with a high energy barrier.

The calculated rates for the second regime were used to compute activation energies with the Arrhenius equation:

$$\ln k = \ln k_0 - \left(\frac{\Delta E_a}{R}\right)\frac{1}{T} \qquad (3)$$

The logarithmic dependence of the calculated rates on inverse temperature is illustrated in Figure 9b. These plots give activation energies of 82.2 ± 2.1, 73.2 ± 2.4, and 70.6 ± 1.8 kJ/mol for 100%, 95%, and 85% cage occupancy, respectively. The calculated value for 95% occupancy, which corresponds to that of naturally occurring samples,[1] is 8 kJ/mol lower than the experimental value of 81 kJ/mol.[11] This discrepancy most likely reflects an inadequacy in the COS/G2 force field or in the combination rules used to determined the methane−water Lennard-Jones parameters.

The existence of an activation energy for the hydrate decomposition process implies that there is a transition state (or family of transitions states) for decomposition. In this regard, the energy costs required to activate the small and large cages of methane hydrate might be expected to be different.[71,72] Gupta et al.[73] have expressed the view that for this reason an activation-controlled mechanism should result in a change of the ratio of the occupancies of the small and large cages during hydrate decomposition. The NMR studies of these authors showed that the small/large cage occupancy ratio remained constant during dissociation, which they took as indicating that the process is not activation controlled. However, the NMR spectra were recorded at $P = 2.09$ MPa and $T = 269-271$ K, i.e., below the ice point and under a small (2−4 K) driving force for hydrate decomposition (recall that $T_{eq} = 267$ K). Under these conditions the destruction of the hydrate host lattice is most likely controlled by the diffusion of the methane molecules through a porous ice layer.[60] Thus, the NMR measurements do not necessarily rule out an activated process for the decomposition at temperatures above which ice can form.

Panels a−c of Figure 10 show that after closed large cages begin to dissociate, there is a time delay before dissociation of the closed small cages begins (see the pronounced plateaus in the figures). Although this would seem to support a model with different rates of decomposition for the large and small cages, the time delay is, in fact, a consequence of the structure of the hydrate lattice in which the first closed cages exposed to the interface during decomposition are the large cages sharing vertices with corresponding small cages located further inside the crystal lattice (Figure 2). Typically, 16−22 closed large cages decompose before the closed small cages begin to decompose. This is in good agreement with the number (18) of closed large cages at the interface. Since there are almost no occurrences of cage collapse within the hydrate phase during decomposition, it is not surprising that the closed $5^{12}6^2$ cages at the surface dissociate before any closed 5^{12} cages dissociate. When both types of closed cages are dissociating, the rates are indeed found to be different by close to a 3:1 ratio, consistent with the ratio of $5^{12}6^2$ and 5^{12} cages in the hydrate cell. This analysis shows that although the methane hydrate decomposition process is activated, it is not accompanied by a substantial change in the small/large cage occupancy ratio.

Further analysis of the evolution of methane molecules initially residing in closed and open cages reveals unusual behavior at long simulation times (Figure 10). Assuming continuous decomposition of the hydrate crystal, the numbers of methane molecules remaining inside each of the three types of cages (counting the open cages at the surface) should decrease monotonically. This tendency is indeed seen at the beginning of the simulations (Figure 10). However, in many trajectories, the methane population displays oscillatory behavior at times beyond 6 ns, i.e., after a significant portion of the hydrate sample has dissolved (Figure 10b−d). Examination of these trajectories reveals that this behavior is a consequence of water molecules in the liquid phase nucleating around methane molecules, thereby forming partial hydrate cages. This nucleation process occurs in the liquid phase in the vicinity of the moving interface boundary as confirmed by monitoring the z-coordinate of the methane molecules. Visual inspection of the trajectories reveals that these methane molecules become trapped in fluctuating

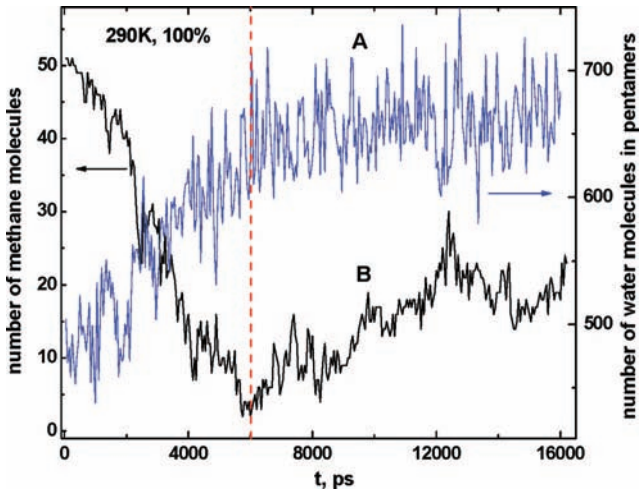

Figure 11. The number of methane molecules in open cages in the hydrate phase at the hydrate/water interface (curve B) and the number of pentamers in the liquid phase (curve A) at $T = 290$ K and 100% cage occupancy vs. time. The dashed line indicates the beginning of reversible crystal regrowth.

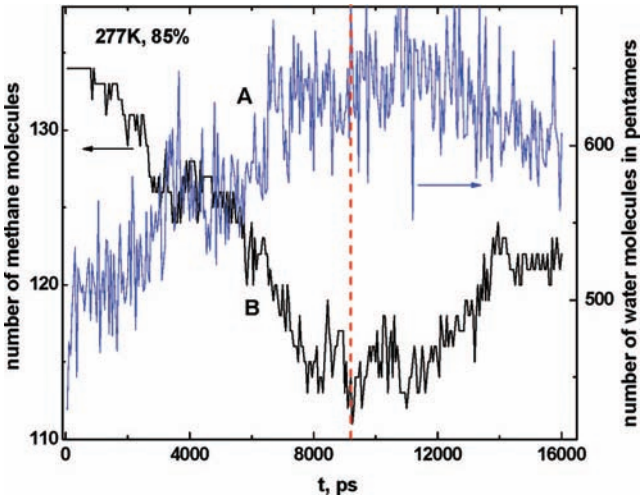

Figure 12. The number of methane molecules in large $5^{12}6^2$ cages of the hydrate lattice (curve B) and the number of pentamers in the liquid phase (curve A), during the course of the simulation at $T = 277$ K and 85% cage occupancy vs. time. The dashed line indicates the beginning of reversible crystal regrowth.

partially open water cages connected to the rest of the dissociating hydrate core. During the course of several hundred picoseconds, some of these cages dissolve, while others grow. In other words, the methane molecules act as nucleation centers of new expanding cages, e.g., Figure 10b, curve "O".

Since the elemental "building block" of the hydrate lattice is the water pentagon, it is instructive to examine the number of pentagonal arrangements of water molecules in the liquid phase as a function of time. From Figures 11 and 12, it is seen that the number of methane molecules associated with the hydrate lattice and the number of pentagonal rings of water molecules in the liquid correlate with each other for times up to about 6 ns for the conditions considered. The beginning of the oscillations in the decomposition rate is accompanied by a reduction in pentagon accumulation in the liquid phase. The rate oscillation is consistent with the theory for crystal growth,[68,69] which explains the maximum crystallization velocity in terms of two factors: namely, the diffusion of molecules (in the present case, methane) and the driving force of supercooling. In a recent study, Kneafsey et al.[12] have observed a dramatic increase in the rate of hydrate formation upon reducing the driving force by either dropping the pressure toward the equilibrium value at the prevailing temperature or raising the temperature toward the equilibrium value at the prevailing pressure. In our simulations, high diffusion rates and supersaturated concentration of methane at the interface allow methane to explore many sites in the liquid, increasing the probability of sampling sites that are favorable for crystal regrowth and promote hydrate cage assembly. As the concentration of pentagons builds up, the probability of cage development grows. However, under the conditions of the simulations, the caged structures in the liquid are unstable, resulting in oscillating behavior in the hydrate decomposition rates. This process is anticipated in experiments and may affect the overall rate of methane hydrate decomposition.[12,13] At present, the source of water pentagons observed in MD studies is not clearly understood. Their accumulation could be provided by hydrate lattice decay or by methane supersaturation at the interface promoting local water structuring. One of the goals of our future research is to elucidate the role of the dissolved guest and of the melted hydrate lattice in the evolution of pentagonal rings of water molecules in the liquid phase.

V. Conclusion

The kinetics and mechanism of methane hydrate thermal decomposition have been studied for 100%, 95%, and 85% occupancy of the hydrate cages. The presence of empty cages substantially destabilizes the hydrate lattice and speeds up the decomposition process. A decrease in cage occupancy from 95% to 85% is calculated to lead up to a 30% increase in the rate of decomposition. Most naturally occurring samples of methane hydrate from permafrost have a cage occupancy near 95%.[1]

At temperatures only slightly above the decomposition temperature, decomposition of the hydrate lattice is not observed for our simulation times, but would be seen if the simulations were run for sufficiently long times. During these short times we do observe diffusion of methane molecules from preexisting open cages. At higher temperatures, the calculated rates display Arrhenius behavior consistent with the presence of barriers associated with cage decomposition. The computed activation energy is in good agreement with an experimental value. The MD simulations reveal that the decomposition rates of the hydrate lattice are constant during the first several nanoseconds and after that demonstrate oscillating behavior. The oscillatory behavior was attributed to reversible regrowth occurring at the interface and accompanied by the increase of water pentagons in the liquid phase. Under conditions of methane supersaturation and substantial involvement of water molecules in pentagonal arrangements, the methane molecules may act as nucleation centers at the interface, even at temperatures above the equilibrium point.

Simulations of hydrate decomposition at a reservoir scale using computational fluid dynamics have recently suggested that hydrate reformation is thermodynamically possible.[16−18] Experimental studies have also shown that the induction time associated with such a process is reduced in the presence of water that has experienced hydrate decomposition.[14,74−76] The residual cyclic water pentamers observed in the present work may be involved in promoting hydrate reformation and should be considered in developing more accurate theoretical descriptions of these macroscale processes.

Experimental studies provide evidence of so-called memory effects, i.e., long-lived residual structures in the liquid phase that promote hydrate reformation.[14,74−76] Such effects are not

presently included in reservoir models, and one of the challenges in the field is the incorporation of such information from atomistic simulations into the macroscale models.

Acknowledgment. This technical effort is a part of the National Energy Technology Laboratory ongoing research in gas hydrates under contract DE-AC26-04NT41817, Subtask 41817.660.01.03. The authors are grateful to Dr. N. English for helpful discussions and for providing his computer code for the geometric hydrate−liquid distinction.

References and Notes

(1) Sloan E. D.; Koh C. A. *Clathrate Hydrates of Natural Gases*, 3nd ed.; CRC Press: Boca Raton, FL, 2008.
(2) Clauusen, W. F. *J. Chem. Phys.* **1951**, *19*, 1425.
(3) von Stackelberg, M.; Müller, H. R. *Z. Electrochem.* **1954**, *58*, 25.
(4) Ripmeester, J. A.; Ratcliffe, C. I.; Tse, J. S. *J. Chem. Soc., Faraday Trans.* **1988**, *84*, 3731.
(5) Boswell, R. *J. Pet. Sci. Eng.* **2007**, *56*, 9.
(6) Moridis, G. J.; Seol, Y.; Kneafsey, T. J. *5th Int. Conf. Gas Hydrates* **2005**, *1004*, 21.
(7) Kowalsky, M. B.; Moridis, G. J. *Energy Convers. Manage.* **2007**, *48*, 1850.
(8) Gonzalez, M. C.; Hughes, R. G.; Civan, F.; Taylor, C. E. In *Advances in the Studies of Gas Hydrates*; Taylor, C. E., Kwan, J. T., Eds.; Kluwer Academic: New York, 2004; p 27.
(9) Taylor, C. E.; Link, D. D.; Elsen, H. A.; Ladner, E. P. In *Advances in the Studies of Gas Hydrates*; Taylor, C. E., Kwan, J. T., Eds.; Kluwer Academic: New York, 2004; p 199.
(10) Kim, H. C.; Bishnoi, P. R.; Heidemann, R. A.; Rivzi, S. S. H. *Chem. Eng. Sci.* **1987**, *42*, 1645.
(11) Clarke, M. A.; Bishnoi, P. R. *Can. J. Chem. Eng.* **2003**, *79*, 143.
(12) Kneafsey, T. J.; Tomutsa, L.; Moridis, G. J.; Seol, Y.; Freifeld, B. M.; Taylor, C. E.; Gupta, A. *J. Petroleum Sci. Eng.* **2007**, *56*, 108.
(13) Moridis, G. J.; Seol, Y.; Kneafsey, T. J. *Studies of Reaction Kinetics of Methane Hydrate Dissociation in Porous Media*, Report LBNL-57298; Lawrence Berkeley National Laboratory: Berkeley, CA, 2005.
(14) Link, D. D.; Ladner, E. P.; Elsen, H. A.; Taylor, C. E. *Fluid Phase Equilib.* **2003**, *211*, 1.
(15) Gupta, A.; Kneafsey, T. J.; Moridis, G. J.; Seol, Y.; Kowalsky, M. B.; Sloan, E. D. *J. Phys. Chem. B* **2007**, *110*, 16384.
(16) Moridis, G. J., Kowalsky, M. B.; Pruess, K. *2005 SPE Annual Technical Conference and Exhibition*, Dallas, TX, October, 9−12, 2005.
(17) Moridis, G. J.; Reagan, M. T. *2007 Offshore Technology Conference*, Houston, TX, April 30−May 3, 2007.
(18) Moridis, G. J.; Collett, T. S.; Boswell, R.; Kurihara, M.; Reagan, M. T.; Koh, C.; Sloan, E. D. *2008 SPE Unconventional Reservoirs Conference*, Keystone, 10−12 February 10−12, 2008.
(19) Rosenbaum, E. J.; English, N. J.; Johnson, J. K.; Shaw, D. W.; Warzinski, R. P. *J. Phys. Chem. B* **2007**, *111*, 13194.
(20) Jiang, H.; Myshakin, E. M.; Jordan, K. D.; Warzinski, R. P. *J. Phys. Chem. B* **2008**, *112*, 10207.
(21) Ota, M.; Qi, Y. *JSME Int. J. Ser. B* **2000**, *43*, 719.
(22) Radhakrishnan, R.; Trout, B. L. *J. Chem. Phys.* **2002**, *177*, 1786.
(23) Báez, L. A.; Clancy, P. *Ann. N.Y. Acad. Sci.* **1994**, *715*, 177.
(24) English, N. J.; MacElroy, J. M. D. *J. Comput. Chem.* **2003**, *24*, 1569.
(25) English, N. J.; Johnson, J. K.; Taylor, C. E. *J. Chem. Phys.* **2005**, *123*, 244503.
(26) Rodger, P. M. In Gas hydrates: Challenges for the Future Holder, G. D., Bishnoi, P. R., Eds. *Ann. N. Y. Acad. Sci.* **2000**, *912*, 474.
(27) Pratt, R. M.; Mei, D.-H.; Guo, T.-M.; Sloan, E. D. *J. Chem. Phys.* **1997**, *106*, 4187.
(28) Rodger, P. M.; Forester, T. R.; Smith, W. *Fluid Phase Equilib.* **1996**, *116*, 326.
(29) Chihaia, V.; Adams, S.; Kuhs, W. F. *Chem. Phys.* **2005**, *317*, 208.
(30) Westacott, R. E.; Rodger, P. M. *Chem. Phys. Lett.* **1996**, *262*, 47.
(31) Westacott, R. E.; Rodger, P. M. *J. Chem. Soc., Faraday Trans.* **1998**, *94*, 3421.
(32) Moon, C.; Taylor, P. C.; Rodger, P. M. *J. Am. Chem. Soc.* **2003**, *125*, 4706.
(33) Førrisdahl, O. K.; Kvamme, B.; Haymet, A. D. *Mol. Phys.* **1996**, *89*, 819.
(34) Nada, H. *J. Phys. Chem. B* **2006**, *110*, 16526.
(35) Ding, L. Y.; Geng, C. Y.; Zhao, Y. H.; Wen, H. *Mol. Simul.* **2007**, *33*, 1005.
(36) Berendsen, H. J. C.; Grigera, J. R.; Straatsma, T. P. *J. Phys. Chem.* **1987**, *91*, 6269.
(37) Kumagai, N.; Kawamura, K.; Yokokawa, T. *Mol. Simul.* **1994**, *12*, 177.
(38) Rick, S. W.; Stuart, S. J.; Berne, B. J. *J. Chem. Phys.* **1994**, *101*, 6141.
(39) Gay, S. C.; Smith, E. J.; Haymet, A. D. J. *J. Chem. Phys.* **2002**, *116*, 8876.
(40) Luo, S.-N.; Strachan, A.; Swift, D. C. *J. Chem. Phys.* **2004**, *120*, 11640.
(41) Yu, H.; van Gunsteren, W. F. *J. Chem. Phys.* **2004**, *121*, 9549.
(42) Tse, J. S.; Klein, M. L.; McDonald, I. R. *J. Chem. Phys.* **1984**, *81*, 6146.
(43) Allen, M. P.; Tildesley, D. J. *Computer Simulation of Liquids*; Clarendon Press: Oxford, UK, 1987.
(44) Ewald, P. P. *Ann. Phys.* **1921**, *64*, 253.
(45) Darden, T.; York, D.; Pedersen, L. *J. Chem. Phys.* **1993**, *98*, 10089.
(46) Essmann, U.; Perera, L.; Berkowitz, M. L.; Darden, T.; Lee, H.; Petersen, L. *J. Chem. Phys.* **1995**, *103*, 8577.
(47) (a) van der Spoel, D.; Lindahl, E.; Hess, B.; van Buuren, A.; Apol, E.; Tieleman, P.; Meulenhoff, P.; Sijbers, A.; Feenstra, A.; Drunen, R.; Berendsen, H. *Gromacs User Manual*, version 3.3.1; www.gromacs.org, 2006. (b) Berendsen, H. J. C.; van der Spoel, D.; van Drunen, R. *Comput. Phys. Commun.* **1995**, *91*, 43. (c) Lindahl, E.; Hess, B.; van der Spoel, D. *J. Mol. Model.* **2001**, *7*, 306.
(48) Parrinello, M.; Rahman, A. *J. Appl. Phys.* **1981**, *52*, 7182.
(49) Nóse, S.; Klein, M. L. *Mol. Phys.* **1983**, *50*, 1055.
(50) Nóse, S. *Mol. Phys.* **1994**, *52*, 255.
(51) Hoover, W. G. *Phys. Rev. A* **1985**, *31*, 1695.
(52) Hayward, J. A.; Reimers, J. R. *J. Chem. Phys.* **1997**, *106*, 1518.
(53) Nada, H.; Furukawa, Y. *J. Cryst. Growth* **2005**, *283*, 242.
(54) Bernal, J. D.; Fowler, R. H. *J. Chem. Phys.* **1933**, *1*, 515.
(55) Sum, A. K.; Burruss, R. C.; Sloan, E. D. *J. Phys. Chem. B* **1997**, *101*, 7371.
(56) Berendsen, H. J. C.; Postma, J. P. M.; DiNola, A.; Haak, J. R. *J. Chem. Phys.* **1984**, *81*, 3684.
(57) Stern, L. A.; Circone, S.; Kirby, S. H. *J. Phys. Chem. B* **2001**, *105*, 1756.
(58) Stern, L. A.; Circone, S.; Kirby, S. H.; Durham, W. B. *J. Phys. Chem. B* **2002**, *106*, 228.
(59) Kuhs, W. F.; Genov, G.; Staykova, D. K.; Hansen, T. *Proc. 5th Int. Conf. Gas Hydrates* **2005**, *1*, 14.
(60) Liang, M.; Chen, G.; Sun, S.; Yan, L.; Lui, S.; Ma, Q. *J. Phys. Chem. B* **2005**, *109*, 19034.
(61) Báez, L. A. Ph.D. Thesis, Cornell University, 1996.
(62) English, N. J. Ph.D. Thesis, University College Dublin, 2003.
(63) Uttormark, M. J.; Thomson, M. O.; Báez, L. A.; Clancy, P. *Mol. Simul.* **1993**, *11*, 121.
(64) www.lsbu.ac.uk/water/phase.html.
(65) Fernandez, R. G.; Abascal, J. L. F.; Vega, C. *J. Chem. Phys.* **2006**, *124*, 144506.
(66) Mahoney, M. W.; Jorgensen, W. L. *J. Chem. Phys.* **2000**, *112*, 8910.
(67) Jiang, H.; Jordan, K. D.; Taylor, C. E. *J. Phys. Chem. B* **2007**, *111*, 6486.
(68) Wilson, H. A. *Philos. Mag.* **1900**, *50*, 238.
(69) Frenkel, J. *Phys. Z. Sowjetunion* **1932**, *1*, 498.
(70) Nicholson, B. F.; Clancy, P.; Rick, S. W. *J. Cryst. Growth* **2006**, *293*, 78.
(71) Jing, M.; Dong, S. *J. Nat. Gas Chem.* **2005**, *14*, 238.
(72) Koyama, Y.; Tanaka, H.; Koga, K. *J. Chem. Phys.* **2005**, *122*, 074503.
(73) Gupta, A.; Dec, S. F.; Koh, C. A.; Sloan, E. D. *J. Phys. Chem. C* **2007**, *111*, 2341.
(74) Natarajan, V.; Bishnoi, P. R.; Kalogerakis, N. *Chem. Eng. Sci.* **1994**, *49*, 2075.
(75) Ohmura, R.; Ogawa, M.; Yasuka, K.; Mori, Y. J. *J. Phys. Chem. B* **2003**, *107*, 5289.
(76) Thomson, H.; Soper, A. K.; Buchanan, P.; Aldiwan, N.; Creek, J. L.; Koh, C. *J. Chem. Phys.* **2006**, *124*, 164508.

JP807208Z